PAPER

Performance of $ZnMn_2O_4/SiO_2$ sorbent for high temperature H_2S removal from hot coal gas

Tzu-Hsing Ko, [iD] *[a] Shumao Wang, [iD] [a] Feng-Hsiang Chang [iD] [b] and Chen-Yao Chu [iD] [c]

A spinel $ZnMn_2O_4$ sorbent supported on SiO_2 was fabricated using a wetness impregnation method for high temperature desulfurization. The operating parameters including operating temperature, $ZnMn_2O_4$ content, space velocity, gas composition, and multiple desulfurization/regeneration cycles were evaluated to understand the optimal condition. The $ZnMn_2O_4/SiO_2$ sorbent exhibits better desulfurization performance when operating temperature is controlled above 600 °C and the suitable space velocity is between 5000–15 000 h^{-1}. The relationship among CO, H_2, and CO_2 on sorbent utilization could be explained *via* the water shift reaction. The sorbent utilization of the $ZnMn_2O_4/SiO_2$ sorbent was retained at approximately 70% after ten desulfurization/regeneration cycles. Elemental analyses demonstrated that the formation of the spinel structure of $ZnMn_2O_4/SiO_2$ improved the Zn stability and no Zn vaporization or loss were observed after ten desulfurization/regeneration cycles. X-ray diffraction (XRD) and temperature programmed regeneration (TPR) were used to characterize the crystal phase and regeneration phenomena of the $ZnMn_2O_4/SiO_2$ sorbent. XRD results demonstrated the presence of spinel structure of $ZnMn_2O_4$, and no Zn and Mn oxides were observed after multiple cycles, indicating that the $ZnMn_2O_4/SiO_2$ sorbent is thermodynamically stable for high temperature desulfurization. Through the EDS and TPR analyses, the residual sulfur was found in the regenerated sorbent and this sulfur species is sulfate from incomplete regeneration. A regeneration temperature of 700 °C was the best choice to overcome the formation of metal sulfate.

1. Introduction

In past years, various metal oxides and modified metals have been widely used as sorbents for hot coal gas desulfurization at high temperatures.[1–6] Among the investigated metal sorbents, studies have primarily focused on Zn oxide (ZnO) and related modified sorbents because they present numerous advantages, such as a favorable thermodynamic property with sulfur species, they are suitable for use at a wide range of operating temperatures, and can reduce the concentration of sulfur species to less than 10 ppm.[7–9] However, the reduction of ZnO and subsequent vaporization of elemental Zn remain a severe problem when the temperature is increased to 650 °C.[10,11] More recently, Mn oxides and Mn-based oxides have attracted considerable attention for high temperature desulfurization.[12–14] The reactivity of Mn-based oxides is higher than that of ZnO, and Mn-based oxides cannot be easily reduced to elemental Mn during hot coal gas desulfurization. To overcome

the vaporization of Zn, a series of metals were added with Zn to form alloy sorbents oxides for H_2S removal from hot coal gas. Huang *et al.*[15] prepared Zn–Fe–Mn/MCM-48 sorbent for H_2S removal at 550 °C and the sorbent utilization of 66.1% was achieved. They also indicated that the significant decrease in sorbent utilization after regeneration. It was due to the migration of Zn onto the sorbent surface and Zn accumulated on the surface and vaporized to the exterior from the surface. Guo *et al.*[16] evaluated the regeneration test of Zn–Mn sorbent supported on γ-Al_2O_3 at 400 °C and 600 °C. The results showed that the sulfur capacity decreased with regeneration cycles and over 50% sorbent utilization was loss after nine regeneration cycles for 400 °C and 600 °C due to the destruction of BET surface and pore structure. Furthermore, the previous study revealed that the addition of Mn significantly improves the vaporization of Zn, and it can be used for high-temperature desulfurization. In addition, some crucial operating parameters were obtained and established in the temperature range of 500–700 °C.[17]

It is recognized that supported sorbents have high dispersion of activated species. The mesoporous silica have received much attention because of high surface, large pore volume and uniformly pore size distribution in comparison to TiO_2 and γ-Al_2O_3.[18–21] To our knowledge the preparation and application of Zn–Mn supported on SiO_2 for high temperature desulfurization

[a]Anxi College of Tea Science, Fujian Agriculture and Forestry University, Fuzhou City, 350002, China. E-mail: hsingko@gmail.com

[b]Department of Tourism Affairs, Tzu Hui Institute of Technology, Nanjou Hsian, Pingtung County, Taiwan

[c]Yung-Hsing Financial Workshop Cooperation Company, Kaohsiung, Taiwan

has not been investigated in-depth and incompletely understood. Therefore, in this study, the $ZnMn_2O_4/SiO_2$ sorbent was systematically fabricated using a wetness impregnation method to obtain thermal-stable structure that is widely dispersed on SiO_2. In addition to multiple desulfurization/regeneration cycles, X-ray diffraction (XRD), N_2 adsorption with Brunauer–Emmett–Teller (BET), temperature programmed regeneration (TPR), scanning electronic microscopy equipped with an energy dispersive spectroscopy (SEM/EDS), and elemental analysis were used to elucidate the surface and structure properties of fresh, reacted, and regenerated $ZnMn_2O_4/SiO_2$ sorbent. The experimental results provide a new aspect for the development of new sorbents for high temperature desulfurization.

2. Materials and methods

2.1 Preparation of $ZnMn_2O_4$ sorbent

The $ZnMn_2O_4$ sorbents were prepared by using the wetness impregnation process with an aqueous solutions of $Mn(NO_3)_2 \cdot 4H_2O$ and $Zn(NO_3)_2 \cdot 4H_2O$ as the precursors to form the structure of $ZnMn_2O_4$. Support materials used for the sorbent preparation were pure commercial products SiO_2, TiO_2 and γ-Al_2O_3 which were purchased from Sinopharm Chemical Reagent Company. All the chemical reagents used in this study were analytical grade.

First of all, pure SiO_2, TiO_2 and γ-Al_2O_3 were shattered and sieved to the desired size (50–100 mesh) and dried for 24 h before mixing with metal aqueous solution. For the preparation of $ZnMn_2O_4/SiO_2$ sorbent, 12.4 g of $Mn(NO_3)_2 \cdot 4H_2O$ and 6.1 g of $Zn(NO_3)_2 \cdot 4H_2O$ were added in a 80 mL distilled water. The mixed solution was drop-wise added to 50 g SiO_2 and was dried for 2 h at room temperature followed by drying for one day at 25 °C in an oven. For the preparation of $ZnMn_2O_4/TiO_2$ sorbent, 11.3 g of $Mn(NO_3)_2 \cdot 4H_2O$ and 5.8 g of $Zn(NO_3)_2 \cdot 4H_2O$ were added in a 80 mL distilled water. The mixed solution was drop-wise added to 50 g TiO_2 and was dried for 2 h at room temperature followed by drying for one day at 25 °C in an oven. For the preparation of $ZnMn_2O_4/$γ-Al_2O_3 sorbent, 11.4 g of $Mn(NO_3)_2 \cdot 4H_2O$ and 5.8 g of $Zn(NO_3)_2 \cdot 4H_2O$ were added in a 80 mL distilled water. The mixed solution was drop-wise added to 50 g γ-Al_2O_3 and was dried for 2 h at room temperature followed by drying for one day at 25 °C in an oven. Finally, all the samples were calcined at 700 °C for 2 h in air flow conditions.

2.2 Desulfurization activity performance

Simulative coal-derived gases consisted of 1% H_2S, 25% CO, 15% H_2, and a balance of N_2 from regulation cylinders, which are similar to the quenched exit gas of the popular Kellogg Rust Westinghousecoal gasifier. The gas flow rates were monitored through mass flow controllers. All mass flow controllers were monitored accurately by an infrared soap bubble meter and the concentration of all species were calculated at the condition of standard temperature and pressure. Prior to entering the reactor, the gases were conducted in a mixing pipe to confirm that the mixture gas exhibited turbulent flow. The reactor consisted of a quartz tube, 1.6 cm i.d., 2.0 cm o.d., and 150 cm length, located inside an electric furnace. Quartz fibres were placed in the reactor to support the samples. Two K-type thermocouples were exactly inserted into the reactor near the top and bottom of the samples to measure and control the inlet and outlet temperatures. Prior to the experiment, pure nitrogen gas (purity 99.99%) was fed into the reactor for 30 min at 500 °C to remove adsorbed water and impure materials coated on the surface of the samples. In addition, blank breakthrough experiments were also conducted under the same conditions and it was verified that no reaction occurred anywhere between H_2S and the lines/reactor. The inlet and outlet concentration of H_2S were analysed by an on-line gas chromatograph (HP, GC-5890) equipped with a flame photometry detector (FPD) and fitted with a GS-Q capillary column. A six-port sampling with a 0.5 mL sampling loop was used to sample the inlet and outlet H_2S concentrations. The desulfurization experiment was terminated when the outlet H_2S concentration from the reactor approached the inlet H_2S concentration. After each desulfurization run, the reactor was purged with He gas for 15 min, and regeneration began at 650 °C with 5% O_2. The regeneration experiment was terminated when the SO_2 concentration in the effluent gas was lower than 10 ppm.

2.3 $ZnMn_2O_4$ sorbent characterization

Crystalline structures of the $ZnMn_2O_4$ sorbent before and after desulfurization/regeneration cycles were determined by X-ray powder diffraction (RIGAKU Model D/MAX III–V) with CuKα radiation. The applied current and voltage were 30 mA and 40 kV, respectively. The diffraction patterns were recorded in the angle range $2\theta = 10-80°$ at a scan rate of $3°\ min^{-1}$. The surface area was measured with a Micromeritics ASAP 2010 instrument using adsorption of nitrogen at 77 K. Prior to adsorption measurements, the samples were degassed under vacuum conditions (5 μm Hg) at 100 °C for 2 h. The surface area was calculated by the BET equation. The $ZnMn_2O_4$ sorbents were digested with aqueous aqua regia in a microwave oven. After digestion, filtration, and dilution processes, the extracted solution was analyzed by inductively coupled plasma atomic emission spectrometry (ICP/AES, JY38P model, JOBIN YVON) for determining the Zn and Mn contents.

2.4 Temperature programmed regeneration (TPR) performance

Temperature programmed regeneration (TPR) was performed by a thermogravimetric analysis equipped with differential thermal analysis (TGA/DTA, Perkin Elmer Pyris Diamond model). TPR experiments were conducted in a mixture of 5% O_2 and He. A quantity of 25 mg of the reacted $ZnMn_2O_4$ sorbent was heated from room temperature to 900 °C at a heating rate of $10\ °C\ min^{-1}$. The sample was placed on a quartz-made reactor with a PID control electronic furnace. The gaseous sulfur compounds from the outlet in the TPR were measured and recorded with a gas chromatography (Shimadzu, GC-14B) equipped with a flame photometry detector.

2.5 Scanning electronic microscopy (SEM)/energy dispersive spectroscopy (EDS)

Surface distribution of elements in red soils was obtained by using an EDS technique which employs a Phillip XL-40FEG scanning electron microscope. All the test samples were mounted on the Cu holder and were coated with platinum prior to EDS analysis.

2.6 X-ray absorption spectroscopy (XAS)

Mn K-edge spectra were undertaken on the wiggler beam-line at the National Synchrotron Radiation Research Center (NSRRC) of Taiwan. The electron storage ring operated at the energy of 1.3 GeV and the beam current varied (current of 80–200 mA). A Si (111) double-crystal monochromator (DCM) was used for providing highly monochromatized photo beams with energies 1–9 keV.

2.7 Solid-state nuclear magnetic resonance (SSNMR)

The solid-state ^{29}Si MAS (magic angle spinning) NMR spectra of samples were recorded under 9.4 tesla with operating frequency of 104.2 MHz on a Bruker Avance DSX400 spectrometer. Zirconia rotors were spun in air at 5 kHz. The deconvolution results and regression fitting of ^{29}Si MAS NMR were performed with Gaussian model using Origin 6.0 version software.

2.8 Elemental analysis (EA)

Elementar vario EL III Heraeus CHNOS Rapid F002, equipped with a flash combustion furnace and thermal conductivity detector (TCD) was used for determination of sulfur content after the desulfurization experimental processes.

3. Results and discussion

3.1 Effect of supports

To facilitate the expression of removal efficiency for $ZnMn_2O_4$, the sorbent utilization is used in this study and is defined as the ratio of the experimental breakthrough time and theoretical breakthrough time. The experimental breakthrough time is defined as the time from the beginning of the desulfurization to the point outlet H_2S concentration reached 50 ppm. The theoretical breakthrough time is defined as the time that $ZnMn_2O_4$ is completely reacted with H_2S. The theoretical breakthrough time can be accurately determined based on the contents of $ZnMn_2O_4$ and the mass flow rate of H_2S and the stoichiometric reaction is represented as follows:

$$ZnMn_2O_4 + 3H_2S + H_2 \rightarrow ZnS + 2MnS + 4H_2O \qquad (1)$$
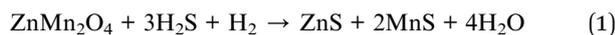
To explore the effect of supports on the high temperature desulfurization, 10 wt% $ZnMn_2O_4$ loading on various supports including SiO_2, TiO_2 and γ-Al_2O_3 were used and the result was shown in Fig. 1. Prior to the experiments performing, the blank, SiO_2, TiO_2 and γ-Al_2O_3 supports were preliminarily tested for their influence on the removal of H_2S and results indicated that no other reactions were observed between H_2S and supports. The influence of removal efficiency for supports can therefore
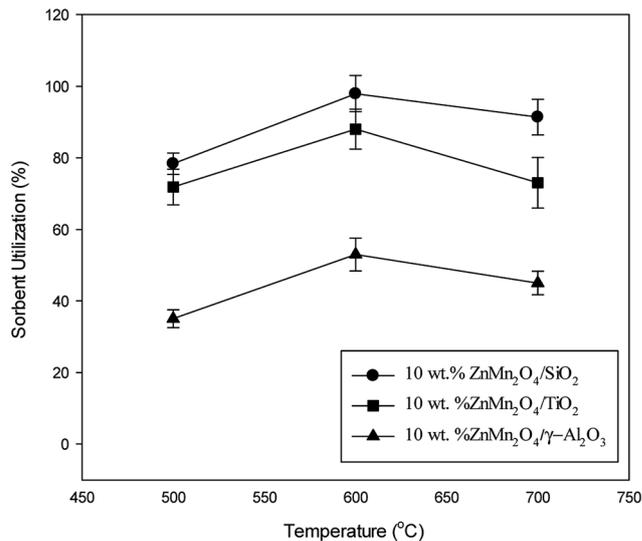

Fig. 1 Sorbent utilization as a function of temperature for $ZnMn_2O_4$ on different supports.

be neglected in this study. As shown in Fig. 1, the SiO_2 is found to have the best sorbent utilization whereas γ-Al_2O_3 appeared to have the worst sorbent utilization. The optimal temperature for all samples was observed at 600 °C. The sorbent utilization slightly decreased when temperature was controlled at 700 °C. Surprisingly, the γ-Al_2O_3 support appeared to have low sorbent utilization. The γ-Al_2O_3 has the largest BET surface area among test supports. A reasonable reason for low sorbent utilization probably associated with the formation of the metal aluminium oxide, $MeAl_2O_4$.[22,23] Although TiO_2 has a moderate sorbent utilization, its thermal stability is a key factor to govern the overall efficiency because of transformation of anatase to rutile/brookite. Temperature exceeded 650 °C is a formation temperature for anatase into rutile form and results in a loss of surface area.[24,25] SiO_2 is a thermal stability material and has been widely used as a support in catalytic field. In this study, SiO_2 has the best sorbent utilization and only a slight decrease in sorbent utilization when temperature is controlled at 700 °C. Therefore, SiO_2 was chosen as a key role for the rest of the experiments.

3.2 Effect of operating temperature

Fig. 2 shows the effect of operating temperature on $ZnMn_2O_4$/SiO_2 utilization under the experimental condition of $T = 400$–750 °C. Experimental results indicate that sorbent utilization increases with operating temperature. The sorbent utilization maintains a stable state when the operating temperature was controlled over 600 °C. No deactivation phenomenon is observed even the operating temperature exceed 750 °C, implying that the addition of Mn improves the vaporization of Zn at high temperature. To understand the contents of Zn and Mn, the fresh and used samples were analyzed with ICP to determine the contents of Zn and Mn. Table 1 shows the contents of Zn and Mn together with recoveries. Note that the recoveries of Zn for all samples are fairly good and no vaporization is found even at 750 °C. This study is motivated to
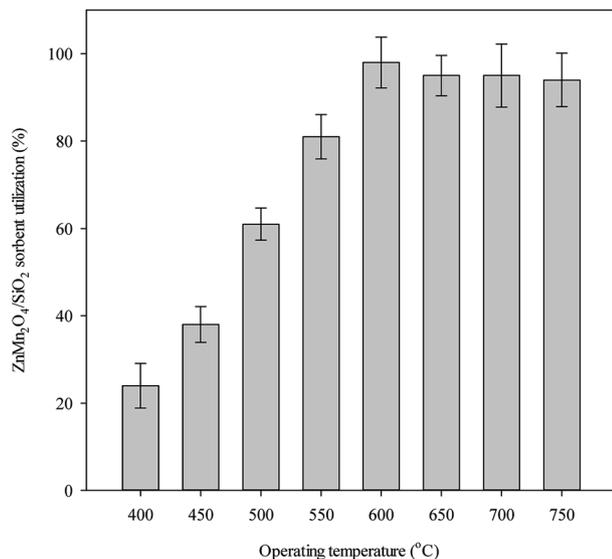
—

Fig. 2 Effect of operating temperature on ZnMn$_2$O$_4$/SiO$_2$ sorbent utilization.

Table 1 Contents of Zn and Mn together with the recovery for various sorbent states[a]

Sorbent state	Contents of Zn, Mn (g kg$_{sorbent}^{-1}$) and sulfur (%)	Recovery (%)
Fresh sorbent	Zn: 26.8	Zn: 98.5
	Mn: 46.3	Mn: 100.4
Reacted sorbent at 600 °C	Zn: 27.3	Zn: 100.4
	Mn: 46.1	Mn: 101.3
	S: 1.97	
Reacted sorbent at 700 °C	Zn: 26.8	Zn: 98.6
	Mn: 44.7	Mn: 97.0
	S: 1.91	
Reacted sorbent at 750 °C	Zn: 27.2	Zn: 100
	Mn: 46.8	Mn: 101.6
	S: 1.89	
Regenerated sorbent	Zn: 27.1	Zn: 99.6
	Mn: 46.7	Mn: 101.3
	S: 0.17	
Regenerated sorbent after 3 cycles	Zn: 27.3	Zn: 100.4
	Mn: 45.7	Mn: 99.1
Regenerated sorbent after 5 cycles	Zn: 27.7	Zn: 101.8
	Mn: 46.5	Mn: 100.9
Regenerated sorbent after 10 cycles	Zn: 27.5	Zn: 101.1
	Mn: 45.8	Mn: 99.3
	S: 0.17	

[a] Preparation concentration of Zn: 27.2 g kg$_{sorbent}^{-1}$, preparation concentration of Mn: 46.1 g kg$_{sorbent}^{-1}$, sulfur content was detected by EA.

evaluate the effectiveness of applying Mn as a promoter to improve the shortcoming of Zn-based sorbent for high temperature desulfurization. Indeed, ZnMn$_2$O$_4$/SiO$_2$ sorbent shows good performance for H$_2$S removal at high temperature. Although it is well known that high temperature enhances the desulfurization efficiency, the equilibrium concentration of H$_2$S is a function of metal oxides and the inlet H$_2$O content. For example, the equilibrium concentration of H$_2$S for the reaction of MnO$_2$ and H$_2$S is 2.5 ppm and 216 ppm at 400 °C and 750 °C (gas composition involved CO: 42.5%, H$_2$: 32.175%, H$_2$O: 12.5%, CO$_2$: 12.5%, H$_2$S: 0.325%). When the operating temperature is controlled at 970 °C with the identical condition, the equilibrium concentration of H$_2$S is 100 ppm.[26] Recent studies have revealed that desulfurization system components become prohibitively expensive as the operating temperature increases and the optimum desulfurization temperature is controlled between 350–600 °C.[27,28] Over such a range of temperatures, the efficiency of the process and its technical viability reduce the overall cost of the process.

3.3 Effect of ZnMn$_2$O$_4$ content

To investigate the effect of ZnMn$_2$O$_4$ content on the removal of H$_2$S, various ZnMn$_2$O$_4$ contents ranging from 5.1–39.2 wt% were carried out in order to understand the optimal preparation content. Fig. 3 exhibits the sorbent utilization as a function of the ZnMn$_2$O$_4$ content. More than 95% sorbent utilization was obviously achieved when the ZnMn$_2$O$_4$ content was controlled less than 14.8 wt%. The sorbent utilization decreased with ZnMn$_2$O$_4$ content and only 60% sorbent utilization is observed for 39.2 wt% content. This implies that the higher sorbent utilization ranging from 5–15 wt% is attributed to a good dispersion of ZnMn$_2$O$_4$ on the SiO$_2$ support. On the other hand, the higher content of ZnMn$_2$O$_4$ enhances the overall removal reaction from the kinetic consideration. The product, metal

sulfides are dense materials, which increase the mass transfer resistance and further repress H$_2$S diffusion into the sorbent core. The sorbent utilizations for 10.2 wt% and 14.8 wt% are close to 100%, however, the breakthrough curve of 14.8 wt% sorbent exhibits a more smooth feature than that of 10.2 wt% sorbent. This is due to the fact that diffusion resistance of H$_2$S through thick sulfide layer increases and reduces the reaction rate of internal oxide. Therefore, 10.2 wt% ZnMn$_2$O$_4$/SiO$_2$ sorbent is considered to be more available for a series of desulfurization reactions.

3.4 Effect of space velocity
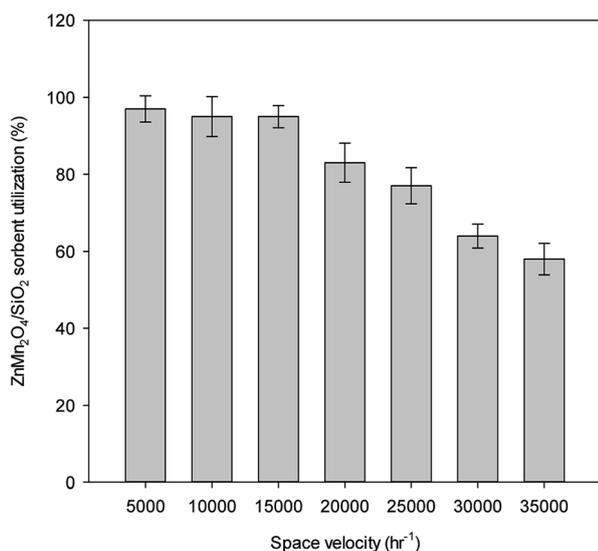
The effect of space velocity on ZnMn$_2$O$_4$/SiO$_2$ utilization is shown in Fig. 4. The operating temperature is controlled at 600 °C and the inlet concentration of gases is fixed at 1% H$_2$S, 25% CO, 15% H$_2$, and a balance of N$_2$. Results indicate that sorbent utilization reaches and maintains at the maximum value of 98% with the space velocity varying from 5000–15 000 h^{-1}. The sorbent utilization is gradually decreased when the space velocity is increased to 20 000 h^{-1}. With the space velocity of 35 000 h^{-1}, the sorbent utilization is further reduced to 60%, which is about 60% of the maximum value. Reduction of sorbent utilization at high space velocity might result from the limitation of diffusion. No significant change in the sorbent utilization within the ranges of 5000–15 000 h^{-1}, suggesting that the external mass transfer resistance can be ignored at this range. Space velocity can be further defined by the phase of the

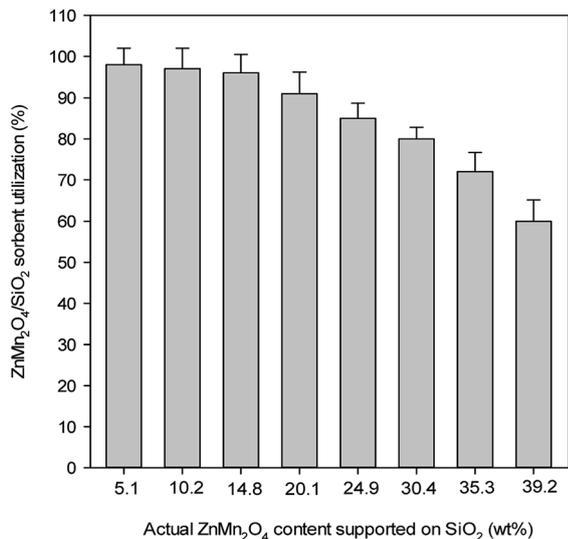
BET surface area, (ii) activated species loss, (iii) uncompleted regeneration. Regeneration is an intense exothermic reaction and the surface and bulk structures of the $ZnMn_2O_4/SiO_2$ sorbent likely underwent a major change because of the exothermic condition. The N_2 adsorption isotherm and pore size distribution for fresh, reacted and regenerated sorbents is shown in Fig. 7. It can be found that all the samples possessed the typical characteristic of type II isotherm according to the IUPAC classification. It indicated that all the sorbents exhibited a uniform ordered macro-pore structure. Furthermore, after desulfurization and regeneration processes the isotherm features have similar with the fresh sorbent, which means that the pore structures did not change too much before and after desulfurization and regeneration. BET surface areas were 86 m^2 g^{-1}, 80 m^2 g^{-1} and 76 m^2 g^{-1} for fresh, reacted, and regenerated sorbents. On the other hand, the sorbent after ten desulfurization/regeneration cycles retained 70 m^2 g^{-1} of BET surface area. As shown in Fig. 7, the fresh sorbent exhibited the smaller pore diameter ranging 10–20 nm, while it ranged from 15–30 nm for the reacted sorbent. The probable reason was that few mesopores maybe collapsed during the high temperature desulfurization or resulted from the formation of metal sulfides because of larger radius of metal sulfides. After regeneration process, a broad feature of pore size distribution is obviously observed. The main pore diameter is in 20–80 nm, which indicated that the regeneration reaction is the major reason to change pore size distribution and is attributed to the exothermic reaction from regeneration. Although BET surface area was found to decrease after reaction and regeneration, it may be one of the reasons to cause sorbents' degeneration because approximately 18% BET surface area was lost after ten successive desulfurization/regeneration cycles. As mentioned, the primary problem of a Zn-based sorbent is the vaporization
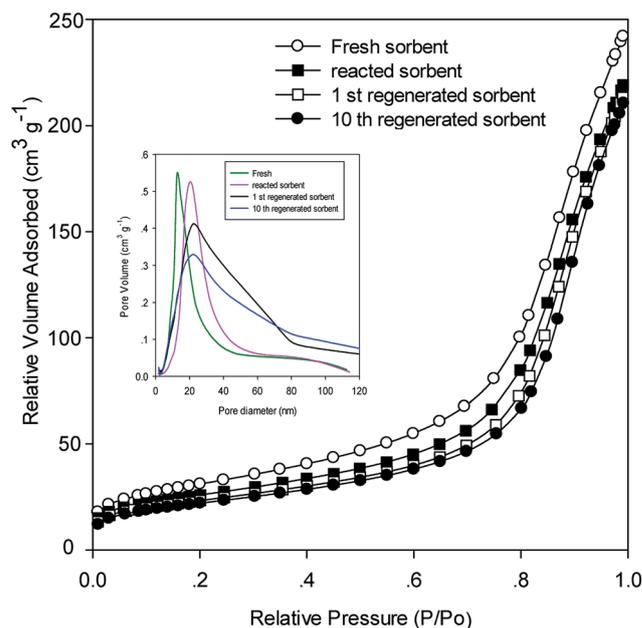

Fig. 7 N_2 adsorption isotherm of 10 wt% $ZnMn_2O_4/SiO_2$ sorbent at different status.

of elemental Zn at 550 °C. The Zn and Mn contents and the recovery (%) of various samples are listed in Table 1. As expected, the recoveries of Zn and Mn were satisfactory, and no vaporization or loss was observed. The sulfur content was measured by EA. The sulfur content were 1.97%, 1.91%, and 1.89% for 600 °C, 700 °C, and 750 °C, respectively which is corresponding to the result of Fig. 2. It is also observed the presence of sulfur after regeneration sorbent. Residual sulfur presence probably came from the incompleted regeneration reaction.
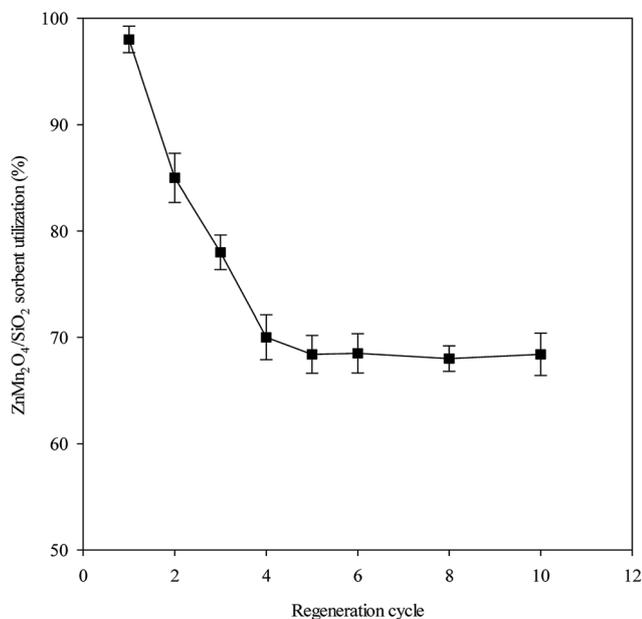
3.7 XRD patterns

XRD was used to understand the changes in the crystal phase of the fresh, reacted and regenerated $ZnMn_2O_4/SiO_2$ sorbents after multiple desulfurization/regeneration cycles. The XRD patterns of various states of sorbents were displayed in Fig. 8. As can be seen that the fresh sorbent has an amorphous structure in which a smooth peak located around at $2\theta = 23°$ is assigned to the SiO_2 support [PDF#39-1425]. On the other hand, the specific peaks at $2\theta = 29.3°$, 33°, 36.4°, and 60.8° were attributed to the reflection of $ZnMn_2O_4$ [PFD#05-0602], implying that all of Zn and Mn were completely reacted to form the spinel structure. No other Si–Zn–Mn oxides were detected, indicating that the interaction between SiO_2 and Zn/Mn can be ignored during calcinations process. After reaction the major peaks were observed at $2\theta = 34.2°$ and 49.2° are ascribed to the diffraction of MnS [PFD#65-0891], whereas $2\theta = 26.9°$, 28.5°, 30.5° and 47.5° are assigned to the reflection of ZnS [PFD#65-0891]. Note that no Zn/Mn oxides were observed after reaction, implying that the spinel structures of $ZnMn_2O_4$ sorbent were completely converted into ZnS and MnS. After regeneration the sorbent possessed the same diffraction pattern in comparison with

Fig. 6 $ZnMn_2O_4/SiO_2$ sorbent utilization as a function of multiple desulfurization/regeneration cycles.

Paper

fresh one. It is noteworthy that the intensity of MnS signals gradually decreased with reaction cycle and was not detected for the reacted sorbent after ten cycles. Previous study prepared Mn-based sorbents for high temperature desulfurization and a series of steam contents were carried out for desulfurization reaction. According to experimental results, the diffraction peaks of MnS weakened with incremental steam content, which showed that the desulfurization reaction was strongly influenced in the atmosphere.[29] Another possible reasons is ascribed to the well dispersed as an amorphous phase or as nano-crystallites after multiple desulfurization/regeneration cycles.[5,30] In addition to the MnS disappearance, an obvious reflection signal at $2\theta = 21.9°$ was assigned to the diffraction of well-crystalline structure of SiO_2 [PFD#46-1045]. The reaction between metal sulfides and O_2 is highly exothermic and accompanying many times of desulfurization/regeneration cycles, an amorphous SiO_2 may result in lattice transformation due to the high temperature rise. The well-crystalline structure of SiO_2 was firstly observed in the regenerated sorbent after three cycles. Although the well-crystalline structure of SiO_2 was formed during regeneration process, there is no change in

the presence of $ZnMn_2O_4$ even after ten desulfurization/regeneration cycle. This result is consistence with the analysis of ICP (shown in Table 1), in which the recoveries of Zn and Mn maintained at least 99%. Ahmed et al.[31] verified that spinel oxides were significantly decomposed and the single metal oxide appeared during the continuous desulfurization/regeneration cycles. From the present results obtained, the formation of $ZnMn_2O_4$ overcame the vaporization of Zn at high temperature.

3.8 XAS and SSNMR identification

The XRD patterns showed the disappearance of MnS and a significant peak of SiO_2 were observed after multiple desulfurization/regeneration cycles. For better understand the fine structure of MnS after multiple desulfurization/regeneration cycles, the reacted, regenerated sorbents after ten cycles, and reference materials were evaluated by the X-ray synchrotron radiation. The extended X-ray absorption fine structure fitting results revealed that the Mn–S bond length was 2.582 Å for the reacted $ZnMn_2O_4$ sorbent. Mn–S bond length for the regenerated sorbent after ten cycles was 2.486 Å, which is longer than that of the reacted sorbent. In addition, we also evaluated the local atomic structure in $Zn_{1-x}Mn_xS$. We found that the Mn–S bond length were 2.415, 2.418 and 2.421 Å for $Zn_{0.88}Zn_{0.12}S$, $Zn_{0.8}Mn_{0.2}S$ and $Zn_{0.67}Mn_{0.33}S$, respectively. Based on our finding, it is speculated that the composition of Mn–S after ten desulfurization/regeneration cycles is a non-stoichiometric structure with zinc. The possible structure of can be expressed as $Zn_{1-x}Mn_xS$, where x ranged from 0.33 to one and maybe present in amorphous phase. In order to understand the structural changes in SiO_2 before and after regeneration in $ZnMn_2O_4$ sorbent, ^{29}Si MAS NMR was measured and fitted by Origin software. Generally, four types of ^{29}Si spectra are identified, namely Q^1, Q^2, Q^3 and Q^4 (Q^n represents the SiO_4 tetrahedron of the amorphous network which forms n bonds with neighboring tetrahedral). The analyses and deconvolution results is tabulated in Table 2. The ^{29}Si spectrum of the fresh $ZnMn_2O_4/SiO_2$ contain a main resonance at around -109.6 ppm corresponding to a trioctahedral structure with four oxygen neighbors and is assigned to the Q^4 structure. The pronounced moderate peak located at -101.6 ppm corresponds to Q^3, $(SiO)_3Si(OH)$ is attached to one hydroxyl group and three Si–O–Si bonds. The signal located at -92.1 ppm is assigned to the Q^2 structure, $(SiO)_2Si(OH)_2$ is bound to two hydroxyl group and two Si–O–Si bonds. The fraction of Q^2, Q^3 and Q^4 are 8.3%, 20.4% and 71.3%, respectively. This implies that the major Si structure in fresh sample is a bulk siloxane group connected with four Si–O–Si bonds. As shown in Table 2, no Q^2 signal was detected and fractions of Q^3 decreased for the regenerated and reacted sorbents after triple and ten cycles. The hydroxyl groups presented in Q^2 and Q^3 gradually disappeared from the crystal lattice of silica oxide because of the extremely heat released from the regeneration reaction at high temperature. The fraction of Q^3 significantly decreased and a fraction of Q^4 increased for regenerated and reacted sorbent after multiple cycles. In fact, the regeneration reaction is a highly exothermic reaction
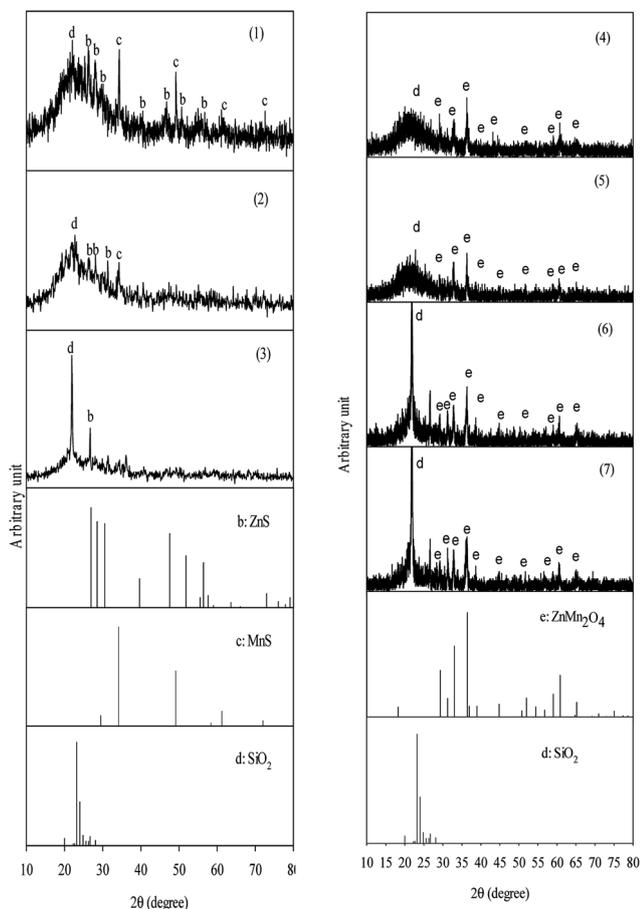

Fig. 8 XRD patterns of the $ZnMn_2O_4/SiO_2$ sorbent in various reactions, (1) reacted sorbent (2) reacted sorbent after three cycles (3) reacted sample after ten cycles (4) fresh sorbent (5) regenerated sorbent (6) regenerated sorbent after three cycles (7) regenerated sorbent after ten cycles.

and it is believed that the highly exothermic reaction leads to the change in ^{29}Si chemical shift. On the basis of XAS and SSMNR, it is summarily concluded that the disappearance of MnS in XRD is probably attributed to the nonstoichiometric structure of $Zn_{1-x}Mn_xS$. On the other hand, the well-crystalline of SiO_2 results from the transformation of spatial structure in lattice.

3.9 TPR analysis

Fig. 9 shows the TPR patterns of the reacted sorbent with a series of MnS, ZnS, $ZnSO_4$, and $MnSO_4$ standard samples. For MnS standard sample, two evident peaks were detected and the first peak located at 400 °C is assigned to the oxidation of MnS to Mn_3O_4. The second one located at 800 °C is due to the formation of $MnSO_4$, which comes from the reaction of MnO_x and SO_2. For ZnS standard sample, two obvious peaks were measured at higher temperature, namely at 625 °C and 850 °C, respectively. They are assigned to the reactions of the oxidation of ZnS to ZnO, and the formation of $ZnSO_4$, respectively. It is remarkable that the formation of metal sulfates during regeneration process. Metal sulfates were undesired by-products, which were inevitably formed due to thermodynamic favorable property with O_2 and may inhibit the diffusion of O_2, thereby restraining the regeneration of the interior region of the sorbent.[32] Unlike metal sulfides, only one peak was obviously detected for both $MnSO_4$ and $ZnSO_4$ standard samples. The peak for $MnSO_4$ and $ZnSO_4$ standard sample is located at 775 °C and 825 °C, respectively. Therefore, it can be concluded that the $MnSO_4$ and $ZnSO_4$ may be decomposed at the temperature higher than of 775 °C and 825 °C. For the reacted sorbent, three major peaks appeared at 400 °C, 625 °C, and 825 °C were detected. This illustrated that the regeneration of the reacted sorbent had three stages. The signal at 400 °C was assigned to the conversion of MnS into Mn_3O_4 whereas the peak at 625 °C was assigned to the conversion of ZnS into ZnO. Note that a small peak appeared at 550 °C was found. The most likely explanation is that the decomposition and oxidation of ZnS that coated on the surface of reacted sorbent. Similar to the second peak, a shoulder peak was also observed at 775 °C and was attributed to the decomposition of $MnSO_4$. There is no doubt that the final peak appeared at 825 °C was assigned to the decomposition of $ZnSO_4$. The regeneration temperature in this study was controlled at 650 °C, which is relatively lower than the
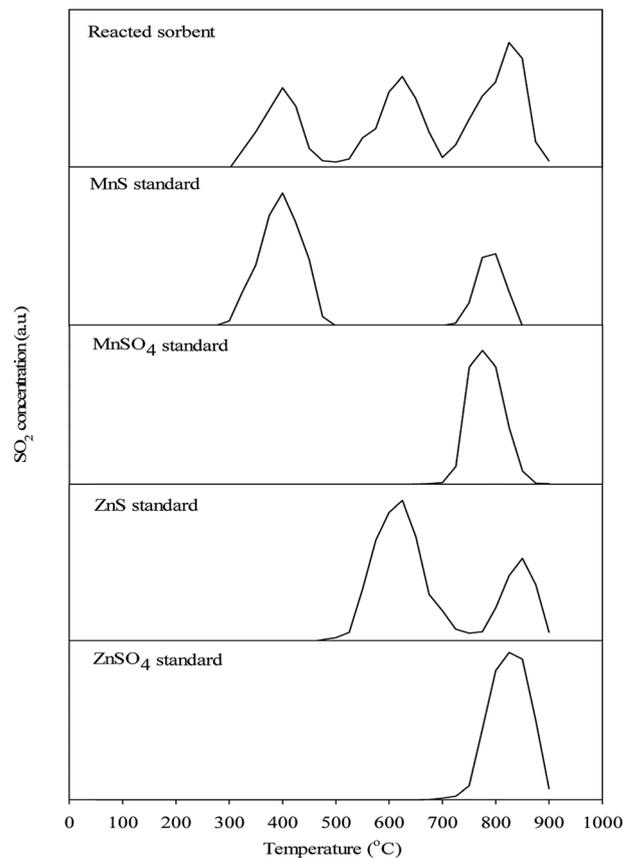

Fig. 9 Temperature programmed regeneration (TPR) patterns of the reacted $ZnMn_2O_4/SiO_2$ sorbent and reference compounds.

requirement of TPR result. In fact, the regeneration is a highly exothermic reaction and actual temperature should be higher than the regeneration temperature. To confirm this viewpoint, the internal temperature of reacted sorbent during regeneration process was experimentally monitored. As expected, although regeneration temperature was controlled at 650 °C, the internal temperature was measured about 780 °C. Unfortunately, the internal temperature of 780 °C appeared too low to complete the regeneration reaction according to the TPR observation and resulted in the presence of metal sulfates due to incomplete reaction.

Table 2 ^{29}Si MAS NMR fitting results and deconvolution of Q^n species for different status of $ZnMn_2O_4/SiO_2$[a]

Sample status	Q^2			Q^3			Q^4		
	FWHM (ppm)	δ (ppm)	I (%)	FWHM (ppm)	δ (ppm)	I (%)	FWHM (ppm)	δ (ppm)	I (%)
Fresh sorbent	8.2	−92.1	8.3	6.4	−101.6	20.4	5.7	−109.6	71.3
Reacted sorbent	9.1	−94.2	5.1	7.0	−101.8	17.5	6.3	−110.3	77.4
Regenerated sorbent (triple cycles)	—	—	—	7.4	−105.2	8.4	6.8	−111.5	92.6
Regenerated sorbent (ten cycles)	—	—	—	7.8	−106.4	4.8	6.9	−112.7	96.2
Reacted sorbent (ten cycles)	—	—	—	7.8	−106.3	5.1	6.6	−112.8	94.9

[a] FWHM, δ and I represent the full width at half maximum, ^{29}Si chemical shift, and relative intensity, respectively. Error value: FWHM ± 0.4 ppm, δ ± 1.5 ppm, I ± 3.6%.
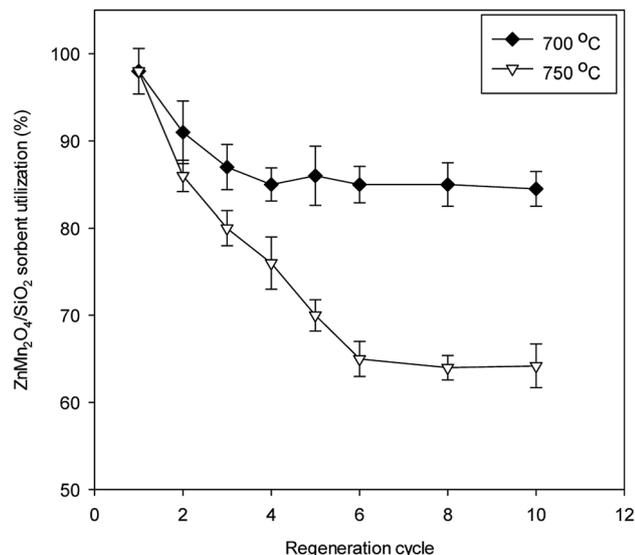
Fig. 10 $ZnMn_2O_4/SiO_2$ sorbent utilization as a function of multiple desulfurization/regeneration cycles at 700 °C and 750 °C.

The TPR result showed that the temperature to complete regeneration reaction for $ZnMn_2O_4/SiO_2$ sorbent should be set at 825 °C. Therefore, two sets of different regeneration temperature were conducted based on the identical condition at the regeneration temperature of 650 °C. Experimental results show that the regeneration temperature of 700 °C appears to have the better sorbent utilization than that of 750 °C (Fig. 10). After sixth desulfurization/regeneration cycles, the sorbent utilization maintain stable state. The stable sorbent utilization for 650 °C, 700 °C, and 750 °C are approximately at 70%, 85%, and 65%, respectively. In addition, the internal temperatures during regeneration process were 843 °C and 876 °C for the regeneration temperature of 700 °C and 750 °C. Note that the higher regeneration temperature (750 °C) cannot achieve the better sorbent utilization after multiple cycles. The internal temperature of 876 °C likely leads to the sintering phenomenon and further results in sorbent degradation due to the loss of surface area. ICP measurements demonstrated that the Zn recovery was 98.5%, which confirms no Zn vaporization during desulfurization/regeneration cycles at the regeneration temperature of 750 °C. However, the surface area decreased by 32 $m^2 g^{-1}$ and small pore structures was distinctly destructed. It is believed that the temperature of 700 °C is the optimal operating choice because of higher sorbent utilization after multiple cycles.

The SEM and EDS images of different sorbents status are shown Fig. 11. The surface of the fresh sorbent was loose and porous. After desulfurization, compact and dense particles were observed on the surface of the reacted sorbent. The sulfur content in the reacted sorbent was estimated about 13.3%, indicating that the H_2S were reacted with $ZnMn_2O_4/SiO_2$ to form metal sulfides (MnS and ZnS). For the regenerated sorbent (after three desulfurization/regeneration cycles) the porous structure was partially restored, which reflected the slight decrease in BET surface. Compared with the fresh sorbent, it is clear observed that the well-crystalline structure appeared after regeneration.
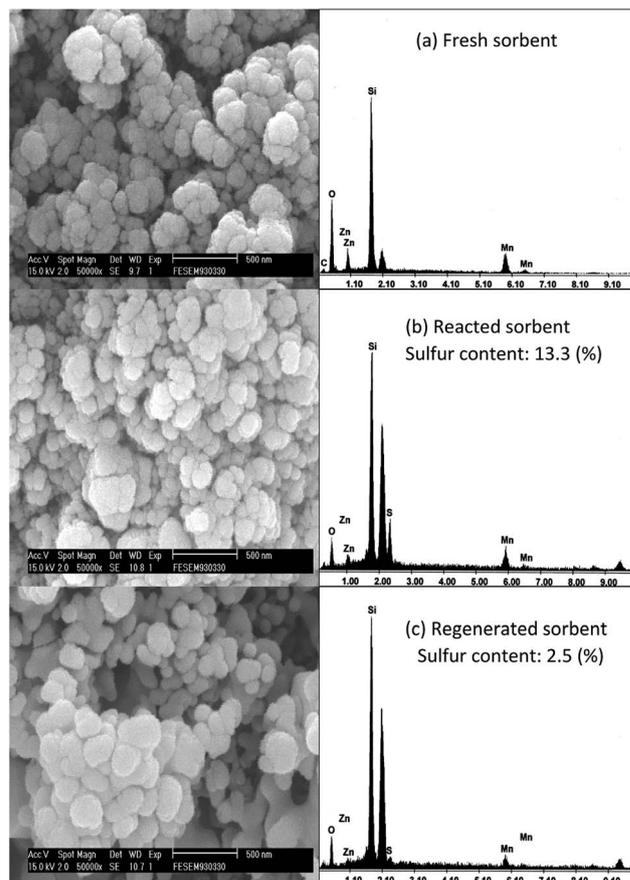

Fig. 11 SEM images and EDS patterns of the (a) fresh (b) reacted (c) regenerated $ZnMn_2O_4/SiO_2$ sorbent.

Furthermore, it can be found that the presence of sulfur in the regenerated sorbent and it may be attributed to the formation of metal sulfates due to incomplete regeneration reaction. According to the results of TPR the one of reasons for the loss of activity of $ZnMn_2O_4$ is the formation of metal sulfate, and an increase in the regeneration temperature is believed to overcome the problem of the formation of metal sulfate.

4. Conclusions

A spinel structure of the $ZnMn_2O_4$ sorbent supported on SiO_2 was fabricated for high temperature desulfurization. Multiple desulfurization/regeneration cycles were conducted to assess the ability of the $ZnMn_2O_4/SiO_2$ sorbent. The $ZnMn_2O_4/SiO_2$ sorbent utilization was retained at 70% and no Zn vaporization was observed after ten desulfurization/regeneration cycles. According to the XRD results, no major changes in the crystal phases occurred after multiple cycles. Through the EA, EDS and TPR analyses, the residual sulfur was found in the regenerated sorbent and this sulfur species is sulphate which resulted by incompleted regeneration. It is suggested that the regeneration temperature of 700 °C should be the best condition and maintains the sorbent utilization at 85% after multiple cycles.

Notes and references

1 S. Cheah, D. L. Carpenter and K. A. Magrini-Bair, *Energy Fuels*, 2009, **23**, 5291–5307.

2 N. R. Jeon, H. S. Song, M. G. Park, S. J. Kwon, H. J. Ryu and K. B. Yi, *Clean technology*, 2013, **19**, 300–305.

3 B. Guo, L. Chang and K. Xie, *Ind. Eng. Chem. Res.*, 2014, **53**, 8874–8880.

4 K. Svoboda, J. Leitner, J. Havlica, M. Hartman, M. Pohorely, J. Brynda, M. Syc, Y. P. Chyou and P. C. Chen, *Fuel*, 2017, **197**, 277–289.

5 H. Xia and B. Liu, *J. Hazard. Mater.*, 2017, **324**, 281–290.

6 K. Y. Chang and E. S. Jae, *Adv. Powder Technol.*, 2010, **21**, 119–124.

7 J. B. Gibson and D. P. Harrison, *Ind. Eng. Chem. Process Des. Dev.*, 1980, **19**, 231–237.

8 M. Mureddu, I. Ferino, E. Rombi, M. G. Cutrufello, P. Deiana, A. Ardu, A. Musinu, G. Piccaluga and C. Cannas, *Fuel*, 2012, **102**, 691–700.

9 V. Girard, D. Chiche, A. Baudot, D. Bazer-Bachi, I. Clemencon, F. Moreau and C. Geantet, *Fuel*, 2015, **140**, 453–461.

10 R. E. Ayala and D. W. Marsh, *Ind. Eng. Chem. Res.*, 1991, **30**, 55–60.

11 T. H. Ko, *Environ. Chem. Lett.*, 2011, **9**, 77–82.

12 J. P. Wakker, A. W. Gerritsen and J. A. Moulijn, *Ind. Eng. Chem. Res.*, 1993, **32**, 139–149.

13 L. Alonso, J. M. Palacios, E. Garcia and R. Moliner, *Fuel Process. Technol.*, 2000, **62**, 31–44.

14 S. Cheah, J. L. Olstad, W. S. Jablonski and M. Bair, *Energy Fuels*, 2011, **25**, 379–387.

15 Z. B. Huang, B. S. Liu, F. Wang and R. Amin, *Appl. Surf. Sci.*, 2015, **353**, 1–10.

16 L. F. Guo, K. L. Pan, H. M. Lee and M. B. Chang, *Ind. Eng. Chem. Res.*, 2015, **54**, 11040–11047.

17 T. H. Ko, H. Chu and Y. J. Liu, *J. Hazard. Mater.*, 2007, **147**, 334–341.

18 S. Lew, A. F. Sarofim and M. Flytzani-Stephanopoulos, *Ind. Eng. Chem. Res.*, 1992, **31**, 1890–1899.

19 J. C. Zhang, Y. H. Wang, R. Y. Ma and D. Y. Wu, *Fuel Process. Technol.*, 2003, **84**, 217–227.

20 J. C. Wang, B. Qiu, L. Han, G. Feng, Y. F. Hu, L. P. Chang and W. R. Bao, *J. Hazard. Mater.*, 2012, **213–214**, 184–192.

21 B. S. Liu, X. N. Wei, Y. P. Zhan, R. Z. Chang, F. Subhan and C. T. Au, *Appl. Catal., B*, 2011, **102**, 27–36.

22 J. Zhang, Y. Wang and D. Wu, *Energy Convers. Manage.*, 2003, **44**, 357–367.

23 J. Wang, B. Liang and R. Parnas, *Fuel*, 2013, **107**, 539–546.

24 R. S. Sonawance, S. G. Hegde and M. K. Dongare, *Mater. Chem. Phys.*, 2000, **77**, 744–750.

25 C. S. Fang and Y. W. Chen, *Mater. Chem. Phys.*, 2003, **78**, 739–745.

26 W. F. Elseviers and H. Verelst, *Fuel*, 1999, **78**, 601–612.

27 R. B. Slimane and J. Abbasian, *Adv. Environ. Res.*, 2000, **4**, 147–162.

28 L. D. Galvin, A. T. Atimtay and R. P. Gupta, *Ind. Eng. Chem. Res.*, 1998, **37**, 4157–4166.

29 Z. B. Huang, B. S. Liu, X. Y. Tang, X. H. Wang and R. Amin, *Fuel*, 2016, **177**, 217–225.

30 K. Polychronopoulou, J. L. G. Fierro and A. M. Efstathiou, *Appl. Catal., B*, 2005, **57**, 125–137.

31 M. A. Ahmed, L. Alonso, J. M. Palacios, C. Cilleruelo and J. C. Abanades, *Solid State Ionics*, 2000, **138**, 51–62.

32 J. Wang, J. Guo, R. Parnas and B. Liang, *Fuel*, 2015, **154**, 17–23.